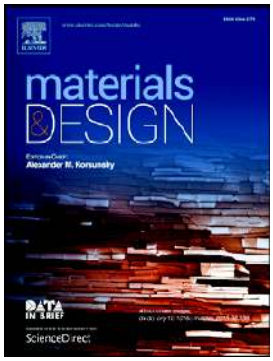

In vitro wear, corrosion and biocompatibility of electron beam melted γ-TiAl

Ashfaq Mohammad, Abdulrahman M. Al-Ahmari, Vamsi Krishna Balla, Mitun Das, Susmit Datta, Devinder Yadav, G.D. Janaki Ram

PII: S0264-1275(17)30742-6
DOI: doi: 10.1016/j.matdes.2017.07.065
Reference: JMADE 3255

To appear in: *Materials & Design*

Received date: 23 November 2016
Revised date: 23 March 2017
Accepted date: 28 July 2017

Please cite this article as: Ashfaq Mohammad, Abdulrahman M. Al-Ahmari, Vamsi Krishna Balla, Mitun Das, Susmit Datta, Devinder Yadav, G.D. Janaki Ram , In vitro wear, corrosion and biocompatibility of electron beam melted γ-TiAl, *Materials & Design* (2017), doi: 10.1016/j.matdes.2017.07.065

In vitro wear, corrosion and biocompatibility of electron beam melted γ-TiAl

Ashfaq Mohammad[1*], Abdulrahman M. Al-Ahmari[2], Vamsi Krishna Balla[3*], Mitun Das[3], Susmit Datta[3], Devinder Yadav[5], G.D. Janaki Ram[4]

[1]FARCAMT Chair, Advanced Manufacturing Institute, King Saud University, Riyadh 11421, Saudi Arabia.

[2]FARCAMT Chair, Advanced Manufacturing Institute, Industrial Engineering Department, College of Engineering, King Saud University, Riyadh 11421, Saudi Arabia.

[3]Bioceramics & Coating Division, CSIR-Central Glass & Ceramic Research Institute (CGCRI), 196, Raja S. C. Mullick Road, Kolkata 700032, India.

[4]Department of Metallurgical and Materials Engineering, Indian Institute of Technology Madras, Chennai 600036, India.

[5]Department of Materials Engineering, Indian Institute of Science, Bangalore, 560012, India.

* Corresponding Authors

Vamsi Krishna Balla

Bioceramics and Coating Division

CSIR-Central Glass & Ceramic Research Institute (CGCRI)

196, Raja S. C. Mullick Road, Kolkata-700032, India.

Fax: +91-33-24730957 Tel. No.: +91-033-24294179

E-mail: vamsiballa@cgcri.res.in

Ashfaq Mohammad

FARCAMT Chair

Advanced Manufacturing Institute

King Saud University, P. O. Box 800

Riyadh 11421, Saudi Arabia.

Tel: +966 14697372. Fax: +966 14678657

E-mail: mashfaq@ksu.edu.sa, ashfaq007@gmail.com

Abstract

Electron beam melting (EBM), a powder bed fusion based additive manufacturing process, has been used to fabricate Ti-48Al-2Cr-2Nb γ-TiAl samples. The samples were evaluated for their potential use in biomedical applications in terms of *in vitro* wear, corrosion and biocompatibility in as-deposited (AD) and hot isostatically pressed (HIPed) conditions. The samples were found to exhibit a lamellar microstructure consisting of γ-TiAl and Ti_3Al (α_2) phases in both the conditions. However, their *in vitro* wear and corrosion performance in Hank's balanced salt solution (HBSS), with and without fetal bovine serum (FBS), was found to be very different. The AD samples exhibited comparable passive behavior to commercially pure titanium (CP-Ti). Their corrosion potentials and currents were better than those of CP-Ti. The γ-TiAl samples exhibited wear rates of the order of 10^{-4} mm^3/N.m in HBSS. The presence of FBS was found to increase the corrosion and the wear rate of this alloy increased by 65%. *In vitro* cell culture experiments, using NIH3T3 cells, demonstrated that the EBM processed γ-TiAl is non-toxic and can allow cell adhesion and proliferation as effectively as CP-Ti.

Keywords: Additive manufacturing; Electron beam melting; Titanium aluminide; Wear; Corrosion; Biocompatibility;

1. Introduction

Gamma titanium aluminides (γ-TiAl) are primarily designed and developed for aerospace applications and possess excellent creep and oxidation resistance and high elastic modulus. Because of their low density (3.8 g/cc), high strength, and good corrosion resistance in body fluids, they are candidate materials for bone implant applications as well. Escudero et al. [1] were the first to consider γ-TiAl for biomedical applications. Using *in vitro* corrosion tests in Ringer's solution, they showed that a γ-TiAl alloy of nominal composition Ti-45Al-2W-0.6Si-0.7B (all compositions are in at.%, unless otherwise specified) possessed superior corrosion resistance than α-β titanium alloy Ti-6Al-4V, a material widely used for biomedical implants. Similarly, two different Ti_3Al-based alloys, Ti-15Al and Ti-13.4Al-29Nb (wt.%), have also been evaluated in Hank's balanced salt solution (HBSS) [2]. The former was found to exhibit better overall corrosion resistance, although the latter showed a wider passivation range due to the

presence of Nb. Following these investigations, preliminary *in vivo* bone-tissue reactions of γ-TiAl alloy Ti-48Al-2Cr-2Nb have been reported by Castaneda-Munoz et al. [3]. Rivera-Denizard et al. [4] studied the *in vitro* biocompatibility of the same alloy using human fetal osteoblast cells and observed comparable cell attachment and growth to alloy Ti-6Al-4V. They also reported that the γ-TiAl alloy did not affect the normal functions of these osteoblast cells. Further, this alloy has also been shown to exhibit comparable corrosion resistance in Ringer's solution to alloy Ti-6Al-4V [5]. Several surface modification techniques such as thermal oxidation, plasma electrolytic oxidation, and micro arc oxidation have been attempted to further improve *in vitro* cell-material interactions and corrosion resistance of γ-TiAl alloys. Thermal oxidation of Ti-45Al-2W-0.6Si-0.7B alloy in air, at 700°C for 24 h, was found to reduce the Al and Ti ion release (in Ringer's solution) by two orders of magnitude when compared to alloy Ti-6Al-4V [1]. Similarly, surface oxidation at 500°C for 1 h in air was found to significantly improve the corrosion resistance of Ti-48Al-2Cr-2Nb alloy [5]. The oxide layers, consisting a mixture of Ti, Al, Cr, and Nb oxides, resulting from thermal oxidation of this alloy were also shown to improve adhesion and proliferation of human osteoblast cell line (hFOB 1.19) [6]. Very recently, further improvement in bone cellular activities such as differentiation has been reported for a γ-TiAl alloy after micro arc oxidation [7]. Plasma electrolytic oxidation has also been used to create bioactive rutile and anatase surface with submicroscopic pores on Ti-48Al-2Cr-2Nb alloy with an aim to improve its osseointegration properties [8].

Earlier investigations focused on biological properties of γ-TiAl alloys clearly demonstrate their strong potential for biomedical implant applications. However, because of their poor ductility at room temperature, it is rather difficult to produce complex-shaped implants out of these alloys employing conventional manufacturing processes. Therefore, manufacturing approaches to create net shape components are to be developed to maximize the utilization of γ-TiAl alloys in biomedical applications. In this context, additive manufacturing (AM) holds great promise, wherein a part is fully automatically produced layer-by-layer directly from its computer aided design (CAD) model without using any part specific tooling. AM of γ-TiAl alloys has already been reported using electron beam melting (EBM) [9–16], selective laser melting [17,18] and laser metal deposition (LMD) [19,20]. Considerable research has been done on EBM of these difficult-to-process alloys. Murr et al. [9] performed microstructural characterization of EBM

fabricated Ti-48Al-2Cr-2Nb coupons. The EBM processing ensured high microstructural homogeneity, purity, minimal defects and consistent room temperature tensile properties [10]. Open cell γ-TiAl foams were also successfully fabricated using EBM [11]. Further, Schwerdtfeger et al. [12] have shown that the microstructure of Ti-48Al-2Cr-2Nb alloy can be tailored from fully lamellar (γ-TiAl/α_2-Ti_3Al) to massive γ-TiAl by controlling the EBM process parameters. A few other γ-TiAl alloys such as Ti-45Al-7Nb-0.3W have also been successfully processed using EBM [13]. These investigations show that the capabilities of EBM can be effectively utilized to fabricate complex-shaped components in γ-TiAl alloys. However, within our knowledge, no attempts have been made so far to evaluate the tribological, corrosion and biological properties of EBM processed γ-TiAl. Therefore, in the present investigation, several Ti-48Al-2Cr-2Nb alloy samples were fabricated using EBM. Some of the samples were subjected to hot isostatic pressing (HIPing). Detailed microstructural, tribological, electrochemical, and biological studies were carried out on both as-fabricated and HIPed samples.

2. Materials and Methods

2.1 Electron beam melting

In the present investigation, γ-TiAl powder (Arcam AB, Sweden) with a nominal composition of Ti-48Al-2Cr-2Nb was used. The powder particles were in the size range of 45 µm to150 µm and the mean particle size of the powder was 110 µm. EBM experiments were conducted using an Arcam A2 machine (Arcam AB, Sweden) and the powder bed was preheated to 1100°C using a beam scanning rate of 8000 mm/s and a beam current of 20 mA. Samples (Z15×X15×Y5 mm) were built using 60 kV acceleration voltage, 25 mA beam current, 1200 mm/s scan speed and 0.2 mm beam offset. Every alternate layer the scan orientation was changed by 90°. Some of the samples were subjected to HIPing at 1200°C for 4 h using argon at 100 MPa. All testing and characterization was performed on the sample surfaces parallel to the build direction (ZX).

2.2 Microstructural and phase analysis

The samples were prepared for microstructural examination following standard metallographic procedures and etched using 100 ml HNO_3, 100 ml HF, and 300 ml H_2O solution. To investigate the grain structure and orientation in the EBM samples, electron backscatter diffraction (EBSD)

analysis was carried out. For EBSD, metallographically prepared samples were further electro-polished using Electrolyte A2 (78 ml perchloric acid, 730 ml ethanol, 100 ml butoxyethanol, and 92 ml distilled water) at 10-12 V and -10°C. EBSD scans performed on an FEI-Inspect-F FEG SEM (FEI Oregon, USA) using a step size of 200 nm. The accelerating voltage and the probe current used were 20 kV and 50 µA, respectively. Grain mapping and texture analysis were carried out using TSL-OIM Analysis 5.2 software. For phase analysis, X-ray diffraction was performed using a Siemens D500 Krystalloflex X-ray diffractometer with Cu-Kα radiation at 30 kV. Vickers microhardness measurements were carried out using 300 g load applied for 15 s. The as-received powder was mounted in Bakelite using a hot mounting press. The mount was metallographically polished until some of the powder particles intersected the surface. Microhardness measurements were then conducted on relatively larger powder particles. At least ten measurements were made on each sample and the average value was reported.

2.3 In vitro wear and corrosion testing

To ensure identical surface roughness, all samples were ground and polished before wear and corrosion testing. Rotating ball-on-disk wear tests were performed using a tribometer (NANOVEA, Microphotonics Inc., CA, USA) and ∅ 3 mm Al_2O_3 ball was used as the counter material. All tests were carried out for 1000 m, in freshly prepared Hank's balanced salt solution (HBSS), at 37±1°C using 5 N normal load and 40 mm/s sliding speed. Identical tests were also performed in HBSS supplemented with 10% fetal bovine serum (FBS) to simulate actual physiological environment. Each test was performed three times on each sample and the average wear rate was calculated from the measured values of wear track width and depth using a contact profilometer. The worn surfaces were examined using scanning electron microscope (SEM) (Phenom proX, Phenom-World B.V., Netherlands) to identify the wear mechanisms.

In vitro corrosion tests were performed in HBSS with and without 10% FBS using a potentiostat/galvanostat (SP300, Bio-Logic SAS, France). A saturated calomel electrode (SCE) and a platinum mesh were used as the reference electrode and the counter electrode, respectively. Prior to current measurements, the system was allowed to idle for 30 min to reach a steady-state condition at the open-circuit potential (OCP). Then the potential was increased at 10 mV/min, starting from – 0.25 V vs. OCP to + 1.6 V. The corrosion potential (E_{corr} vs. SCE) and the

corrosion current (I_{corr}) were obtained from Tafel extrapolation plots. After testing, the sample surfaces were examined using SEM.

2.4 In vitro cell-material interactions

In vitro cell interactions with the EBM processed γ-TiAl sample surfaces were assessed in terms of cytotoxicity using MTT enzymatic assay and cell morphology using SEM. A mouse embryonic fibroblast cell line (NIH3T3) was used in the present work. All cell culture experiments were performed on triplicate samples. Commercially pure titanium (CP-Ti) was used as control. The samples were ground and polished followed by sterilization in an autoclave at 121°C for 30 min. Each sample was placed in a 6-well plate and seeded with 1×10^4 cells/well. The *in vitro* cytotoxicity of γ-TiAl samples, in as-deposited and hot isostatically pressed (HIPed) conditions, was assessed using MTT [3-(4,5-dimethylthiazol-2-yl)-2,5-diphenyl tetrazolium bromide] assay following standard protocol reported elsewhere [21]. Similarly, SEM examination was carried out to assess how the cells adhered and proliferated on different sample surfaces. The procedure described in [21] was followed for cell fixation. The MTT assay and morphology of the cells was observed after 3, 5 and 7 days of culture. Statistical analysis was performed using Student's t-test on MTT assay data and $p < 0.05$ was considered statistically significant. The data is presented as mean ± standard deviation of three independent experiments (n = 3, five measurements from each experiment).

3. Results and Discussion

3.1 Microstructures

Typical microstructures of the EBM processed γ-TiAl alloy Ti-48Al-2Cr-2Nb are shown in **Fig. 1**. In both as-deposited (AD) and HIPed conditions, the alloy showed a predominantly lamellar microstructure. However, the width of the lamella as well as the grain size was noticeably higher in the HIPed samples. The relative density of the EBM processed samples, measured using Archimedes' method, marginally increased from ~ 99% in as-deposited condition to about 99.7% after HIPing. The EDX analysis, presented in **Table 1**, did not reveal any significant differences in the chemical composition between the EBM processed samples and the starting γ-TiAl powder.

The pole figures and EBSD maps of the EBM samples in AD and HIPed conditions (parallel to the build direction, ZX) are presented in **Fig. 2**. Both the samples showed a nearly random texture and no texture differences were observed between the two samples. However, some differences in terms of grain size and grain boundary misorientation angle were observed, as summarized in **Table 1**. Our study showed a significant increase in the fraction of high-angle boundaries after HIPing. The fraction of boundaries with misorientation angle ≥ 15° was 0.55 in the AD samples, while it was 0.86 in the HIPed samples (**Table 1**). The increase in the fraction of high-angle grain boundaries was further supported by concomitant increase in the fraction of Σ3 boundaries (from 0.31 to 0.51) in the HIPed samples. The high fraction of low-angle grain boundaries (0.45) in the AD samples could be due to the growth of γ-TiAl dendrites in slightly different directions in each of the melted tracks [22]. The dendrite growth direction is also influenced by the geometrical shape of the melt pool during EBM [23,24]. In general, the low-angle boundaries have lower mobility than the high-angle boundaries because of their lower energy. Consequently, the high-angle boundaries grow rapidly at the expense of the low-angle boundaries during HIPing. Another reason for the increase in the fraction of high-angle boundaries in the HIPed samples is annihilation/absorption of dislocations generated during EBM processing. This is evident from dislocation maps presented in **Fig. 2c and Fig. 2d**, which reveal relatively more dislocation-free regions in the HIPed samples. The grain size (D90) was found to be ~ 18 μm and ~ 22 μm in AD and HIPed conditions, respectively. Thus, HIPing did not cause any serious grain coarsening in the EBM processed γ-TiAl samples.

The X-ray diffractograms of all the γ-TiAl samples showed distinct peaks corresponding to γ-TiAl and Ti_3Al (α_2) phases, as shown in **Fig. 3**. The samples in AD and HIPed conditions showed very similar peak intensities of γ-TiAl and Ti_3Al (α_2) phases, suggesting that their phase constitution is very similar. However, the feedstock powder was found to contain relatively higher amount of Ti_3Al (α_2) phase as compared to the EBM processed samples. During EBM of γ-TiAl, the microstructural evolution can be expected to take the following sequence. The alloy begins to solidify with the formation of β (bcc solid solution), but completes solidification as single-phase α (hcp solid solution) through a peritectic reaction ($L + \beta \rightarrow \alpha$) [25]. Subsequently, as the alloy cools below the α-transus temperature, some γ phase forms. Finally, upon reaching the eutectoid temperature, the remaining α transforms to a lamellar mixture of $\gamma + \alpha_2$ [26]. Note

that the preheat temperature used in this work (1100°C) is just below the eutectoid transformation temperature of the alloy. Because of the high preheat temperature, the cooling rates in EBM can be expected to be low enough to allow enough time for the various phase transformations to take place to their near completion. Overall, at the end of scanning for each new layer, the newly formed layer develops a microstructure consisting of a lamellar mixture of $\gamma + \alpha_2$ along with some pro-eutectoid γ. When the next layer is generated, the previously deposited layer is reheated into the α phase field, which upon cooling, once again, transforms into pro-eutectoid γ and $\gamma + \alpha_2$ eutectoid mixture. It may be noted that the cooling rate experienced by the material during this reheat thermal cycle is lower than the cooling rate experienced by a layer of material when it was freshly added. Consequently, the scale of the microstructure (width of the eutectoid lamellae) as well as the amount of the pro-eutectoid γ may slightly increase. During HIPing at 1200 °C, the alloy is taken into $\alpha + \gamma$ phase field and the long soaking time equilibrate the phase fractions. Subsequently, as the alloy is slowly cooled from HIPing temperature, some pro-eutectoid γ forms and the remaining α undergoes eutectoid transformation to a lamellar mixture of $\gamma + \alpha_2$ phases. Because the cooling rate in HIPing is much slower than that in EBM processing, the HIPed samples, however, develop a relatively coarser lamellar structure. In essence, it can be seen that the HIPing treatment did not significantly alter the microstructure of the EBM processed γ-TiAl samples. In fact, in microhardness measurements (**Table 1**), the AD and the HIPed samples showed the same average hardness (370 HV). However, the feedstock powder exhibited considerably higher hardness (431 ± 13 HV) than the EBM processed samples. This can be attributed to the higher amount of α_2 phase, which is harder than γ phase, in the feedstock powder [27].

3.2 In vitro corrosion and wear performance

In general, all the γ-TiAl samples showed very a similar variation in the open-circuit potential (OCP) as a function of time up to 3600 s (data not shown here). Upon immersion in HBSS, with or without FBS, the potentials moved sharply towards noble potential and attained stability within 600 s for both AD and HIPed γ-TiAl samples. In comparison, the CP-Ti control samples took ~ 2000 s for attaining a stable potential. These observations suggest that the EBM processed γ-TiAl samples quickly passivate – in fact, faster than CP-Ti – upon immersion in HBSS, with or without FBS. The Tafel curves of the EBM processed γ-TiAl and the CP-Ti control samples are

shown in **Fig. 4**. From these curves, the CP-Ti samples can be seen to exhibit stable passivity with no active region in HBSS, with or without FBS. A similar behavior was displayed by the AD γ-TiAl samples in HBSS with FBS. However, after HIPing the γ-TiAl samples lost their stable passivation behavior and showed an active region in both the solutions. The corrosion potential (E_{corr}), corrosion current (I_{corr}) and passive range (the difference between the breakdown potential (E_b) and the zero current potential (ZCP), see **Fig. 4a)** determined from the Tafel plots are summarized in **Table 2**. The CP-Ti samples, in HBSS with or without FBS, and the AD γ-TiAl samples, in HBSS with FBS, did not show passivity breakdown up to 1.6 V. Therefore, the exact passive range for these samples could not be determined under the present experimental conditions. In AD condition, the EBM processed γ-TiAl samples showed a passive range of 1221 mV (E_b = 1039 mV). In contrast, the HIPed γ-TiAl samples exhibited a passive range of 914 mV in HBSS (E_b = 827 mV) and the addition of 10% FBS decreased the passive range further to 458 mV (E_b = 196 mV). Therefore, it can be concluded that HIPing is detrimental to the passive behavior of EBM processed γ-TiAl, especially in the presence of FBS.

In general, the EBM processed γ-TiAl samples showed relatively higher E_{corr} and lower I_{corr}, hence better corrosion resistance, than the CP-Ti control samples in HBSS. When tested in HBSS, the HIPed γ-TiAl samples showed the noblest E_{corr} of – 87 mV vs SCE, although the AD γ-TiAl samples exhibited the lowest I_{corr} of 0.002 μA. This implies that the HIPed samples offer better resistance to the initiation of corrosion, but the AD samples display a relatively lower corrosion rate. When the HBSS was supplemented with 10% FBS, the corrosion potentials of these samples became less noble suggesting an increase in their corrosion susceptibility. It is well known that proteins/biomolecules such as FBS adsorb onto the sample surfaces [28,29] and alter the surface interactions. For example, the adsorbed layer can act as a diffusion and mass transport barrier influencing the corrosion potentials [30]. The effect depends on the amount of adsorbed protein, continuity of the film, type of the protein and the composition of alloy. Many materials of interest to biomedical industry have been reported to exhibit inferior corrosion resistance in the presence of biomolecules/proteins [30–33]. From the present experimental results, it is very difficult to identify the processing condition of γ-TiAl alloy which would provide the best *in vitro* corrosion resistance. Therefore, Grey relational analysis [34,35] has been performed to combine the effects of E_{corr} and I_{corr} into a single parameter. For normalization

of the responses, the criteria used was 'higher the better' for E_{corr} and 'lower the better' for I_{corr} and wear rate. The best sample is the one that obtains the highest grade (Grey relational grade, G, in Table 3). The analysis, shown in **Table 3**, indicates that the EBM processed γ-TiAl alloy can provide the best *in vitro* corrosion performance after HIPing. This can be substantiated from its high E_{corr} combined with medium I_{corr} in HBSS and low I_{corr} with medium E_{corr} in HBSS supplemented with 10% FBS.

Fig. 5 shows the surface morphologies of the samples after corrosion testing in HBSS with FBS. The samples tested without FBS showed no visible changes on the surface (not shown here). However, addition of 10% FBS appears to alter the surface reactions significantly. As compared to AD γ-TiAl samples (**Fig. 5a**), the HIPed γ-TiAl samples showed a unique surface morphology (**Fig. 5b**) after corrosion testing in HBSS with 10% FBS. The rough surface morphology of the HIPed samples could be due to the breakdown of the passive layer. This is supported by the narrow passive range (458 mV) measured on these samples in HBSS + 10% FBS solution (**Table 2** and **Fig. 4b**). Further, from the **Fig. 5b**, it can be seen that the corrosion is relatively more severe on γ-TiAl than on Ti_3Al (α_2). The Ti_3Al (α_2) phase was observed to be in relief due to less corrosion/dissolution.

Fig. 6 shows the *in vitro* wear rate of the EBM processed γ-TiAl samples in HBSS, with and without FBS. HIPing was found to have a negligible effect on the *in vitro* wear of EBM processed γ-TiAl alloy Ti-48Al-2Cr-2Nb. In HBSS, the average wear rate of the AD samples was 1.79×10^{-4} $mm^3/N.m$ – practically the same as that of the HIPed samples (1.72×10^{-4} $mm^3/N.m$). As shown in **Fig. 6**, the addition of 10% FBS to HBSS increased the wear rate of the AD and the HIPed samples by 37% (2.45×10^{-4} $mm^3/N.m$) and 65% (2.84×10^{-4} $mm^3/N.m$), respectively. Since the hardness of the AD and the HIPed samples is very similar, the difference in the wear rate of these samples can be related to the influence of corrosion during wear testing. As noted earlier, while the AD samples exhibited stable passivity during corrosion testing in HBSS with FBS, the HIPed samples showed passivity breakdown with a narrow passivation range. Thus, during wear testing, the HIPed samples can be expected to undergo corrosion to a greater extent. This, in turn, increases their wear rate as the corrosion products get easily removed in the wear process. The wear track morphologies of the samples are shown in **Fig. 7**.

The wear tracks on AD and HIPed samples can be seen to be very similar. Both the samples exhibited relatively wide worn grooves when tested in HBSS compared to the samples tested in HBSS with FBS. The only difference between the samples tested in HBSS with and without FBS is that the former appeared to have undergone fatigue induced cracking at the worn groove edges, as shown in **Fig. 7c and 7d**. Overall, the wear track morphologies indicate that the dominant wear mechanism was abrasive in nature. Interestingly no visible corrosion products and features were present on these samples. This could be due to complete removal of the corrosion products by wear. The Grey relational analysis, **Table 3**, indicated that the EBM processed γ-TiAl samples in AD condition provide the best combination of *in vitro* wear and corrosion resistance in HBSS with 10% FBS.

3.3 In vitro cell-material interactions

To eliminate the influence of surface roughness on cell-material interactions, all the samples were polished before tissue culture experiments. After polishing, these samples showed an average surface roughness of 0.06 ± 0.01 μm. The viability of the mouse embryonic fibroblast cells (NIH3T3) on the EBM processed γ-TiAl alloy samples was quantitatively determined using MTT assay. The experiments were also conducted on CP-Ti samples for comparison. The percentage of NIH3T3 cell viability on different sample surfaces after 3, 5 and 7 days of culture is shown in **Fig. 8**. Statistical analysis of these results revealed significant differences ($p < 0.05$) in the cell densities among the various samples. The cell viability on AD γ-TiAl samples was always found to be lower when compared to HIPed γ-TiAl samples and CP-Ti control samples. However, the concentration of the cells was found to increase with culture duration on the AD γ-TiAl samples, indicating that the samples are non-toxic and can promote cell proliferation. On the HIPed γ-TiAl samples, however, it was observed that the cells proliferated rapidly. Among all the samples, the HIPed γ-TiAl samples showed the best cell viability over the entire culture duration. It is possible that the high energy associated with the high-angle boundaries, which were in abundance in the HIPed samples facilitated favorable cell-material interactions leading to rapid cell proliferation. The difference in the cell densities of the AD and the HIPed samples decreased gradually with increase in culture time, indicating that the AD samples also promoted cell proliferation although at a lower rate.

The *in vitro* cell interactions with the samples, in terms of cell attachment and spreading, were assessed using cell morphologies. **Fig. 9a** shows the cell morphologies on different samples after 3 days of culture. Although small in number, the cells on the samples showed clear filopodia extensions adhering to the sample surface and cell-to-cell contacts demonstrating that all the samples enabled early-stage cell adhesion, which can lead to spreading and mineralization with time. The cell number and the number of cell-to-cell contacts increased with culture duration as shown in **Fig. 9b and 9c**. None of the samples showed cells with rounded morphology. These characteristics indicate that the cells were well attached to the surfaces and were able to spread. The fibroblast cells were found to form a confluent layer covering the entire surface of the HIPed γ-TiAl samples after 7 days of culture. This demonstrates that these samples are highly biocompatible and provide superior surfaces for the cell adhesion and growth. On the AD samples, the cells were adhered well with microextensions connecting other cells and the substrate, as shown in **Fig. 9c**. Similar cell morphologies were also observed on the CP-Ti control samples. Overall, the NIH3T3 cell adhesion and growth on AD γ-TiAl samples is at par with the CP-Ti samples. In HIPed condition, the EBM γ-TiAl samples perform better than the CP-Ti samples.

4. Conclusions

The present work demonstrates that electron beam melting (EBM) is a viable manufacturing route for fabricating complex-shaped biomedical implants in γ-TiAl alloy Ti-48Al-2Cr-2Nb. EBM processed γ-TiAl samples exhibited measurable differences in *in vitro* corrosion, wear and biocompatibility properties depending on their processing condition. Grey relational analysis showed that the corrosion resistance of this alloy, in Hank's balanced salt solution (HBSS) with and without fetal bovine serum (FBS), can be increased after hot isostatic pressing. A corrosion potential (E_{corr}) of – 262 mV vs SCE and a corrosion current (I_{corr}) of 0.005 μA was recorded in HBSS+FBS solution for hot isostatically pressed alloy. However, the wear rate of the alloy increased from 2.45×10^{-4} mm^3/N.m in as-deposited condition to 2.84×10^{-4} mm^3/N.m after HIPing when tested in the presence of FBS. In general, the adsorption of proteins on the surface of γ-TiAl was found to affect its corrosion and wear resistance. Grey relational analysis indicated that EBM processed γ-TiAl alloy provides the best combination of *in vitro* wear and corrosion resistance in as-deposited condition. EBM processed γ-TiAl samples in as-deposited condition

facilitate *in vitro* cell adhesion and growth at par with commercially-pure titanium – after hot isostatic pressing, the EBM processed γ-TiAl samples perform even better.

Acknowledgements

This project was funded by the National Plan for Science, Technology and Innovation (MAARIFAH), King Abdulaziz City for Science and Technology, Kingdom of Saudi Arabia, Award Number (11-ADV1494-02).

References

[1] Escudero ML, Mu□oz-Morris MA, Garc□a-Alonso MC, Fern□ndez-Escalante E. In vitro evaluation of a gamma-TiAl intermetallic for potential endoprothesic applications. Intermetallics 2004;12:253–60. doi:10.1016/j.intermet.2003.10.004.

[2] Choubey A, Basu B, Balasubramaniam R. Electrochemical behavior of intermetallic Ti3Al-based alloys in simulated human body fluid environment. Intermetallics 2004;12:679–82. doi:DOI 10.1016/j.intermet.2004.03.012.

[3] Castaneda-Munoz DF, Sundaram PA, Ramirez N. Bone tissue reaction to Ti-48Al-2Cr-2Nb (at.%) in a rodent model: a preliminary SEM study. J Mater Sci Mater Med 2007;18:1433–8. doi:10.1007/s10856-006-0095-9.

[4] Rivera-Denizard O, Diffoot-Carlo N, Navas V, Sundaram P a. Biocompatibility studies of human fetal osteoblast cells cultured on gamma titanium aluminide. J Mater Sci Mater Med 2008;19:153–8. doi:10.1007/s10856-006-0039-4.

[5] Delgado-Alvarado C, Sundaram P a. Corrosion evaluation of Ti-48Al-2Cr-2Nb (at.%) in Ringer's solution. Acta Biomater 2006;2:701–8. doi:10.1016/j.actbio.2006.05.012.

[6] Bello S a, de Jesús-Maldonado I, Rosim-Fachini E, Sundaram P a, Diffoot-Carlo N. In vitro evaluation of human osteoblast adhesion to a thermally oxidized gamma-TiAl intermetallic alloy of composition Ti-48Al-2Cr-2Nb (at.%). J Mater Sci Mater Med 2010;21:1739–50. doi:10.1007/s10856-010-4016-6.

[7] Santiago-Medina P, Sundaram P a, Diffoot-Carlo N. The effects of micro arc oxidation of gamma titanium aluminide surfaces on osteoblast adhesion and differentiation. J Mater Sci Mater Med 2014;25:1577–87. doi:10.1007/s10856-014-5179-3.

[8] Lara Rodriguez L, Sundaram PA, Rosim-Fachini E, Padovani AM, Diffoot-Carlo N. Plasma electrolytic oxidation coatings on γTiAl alloy for potential biomedical applications. J Biomed Mater Res Part B Appl Biomater 2014;102:988–1001. doi:10.1002/jbm.b.33079.

[9] Murr LE, Gaytan SM, Ceylan a., Martinez E, Martinez JL, Hernandez DH, et al. Characterization of titanium aluminide alloy components fabricated by additive manufacturing using electron beam melting. Acta Mater 2010;58:1887–94. doi:10.1016/j.actamat.2009.11.032.

[10] Biamino S, Penna a., Ackelid U, Sabbadini S, Tassa O, Fino P, et al. Electron beam

melting of Ti-48Al-2Cr-2Nb alloy: Microstructure and mechanical properties investigation. Intermetallics 2011;19:776–81. doi:10.1016/j.intermet.2010.11.017.

[11] Hernandez J, Murr LE, Gaytan SM, Martinez E, Medina F, Wicker RB. Microstructures for Two-Phase Gamma Titanium Aluminide Fabricated by Electron Beam Melting. Metallogr Microstruct Anal 2012;1:14–27. doi:10.1007/s13632-011-0001-9.

[12] Schwerdtfeger J, Körner C. Selective electron beam melting of Ti-48Al-2Nb-2Cr: Microstructure and aluminium loss. Intermetallics 2014;49:29–35. doi:10.1016/j.intermet.2014.01.004.

[13] Tang HP, Yang GY, Jia WP, He WW, Lu SL, Qian M. Additive manufacturing of a high niobium-containing titanium aluminide alloy by selective electron beam melting. Mater Sci Eng A 2015;636:103–7. doi:10.1016/j.msea.2015.03.079.

[14] Denis Cormier, Ola Harrysson, Tushar Mahale HW. Freeform fabrication of titanium aluminide via electron beam melting using prealloyed and blended powders. Res Lett Mater Sci 2007;2007.

[15] Ge W, Guo C, Lin F. Effect of Process Parameters on Microstructure of TiAl Alloy Produced by Electron Beam Selective Melting. Procedia Eng 2014;81:1192–7. doi:http://dx.doi.org/10.1016/j.proeng.2014.10.096.

[16] Beretta S, Filippini M, Patriarca L, Sabbadini S. Analysis of Fatigue Damage Accumulation in TiAl Intermetallics. Key Eng Mater 2013;592–593:30–5. doi:10.4028/www.scientific.net/KEM.592-593.30.

[17] Löber L, Schimansky FP, Kühn U, Pyczak F, Eckert J. Selective laser melting of a beta-solidifying TNM-B1 titanium aluminide alloy. J Mater Process Technol 2014;214:1852–60. doi:10.1016/j.jmatprotec.2014.04.002.

[18] Gussone J, Hagedorn Y-C, Gherekhloo H, Kasperovich G, Merzouk T, Hausmann J. Microstructure of γ-titanium aluminide processed by selected laser melting at elevated temperatures. Intermetallics 2015;66:133–40. doi:10.1016/j.intermet.2015.07.005.

[19] Qu HP, Wang HM. Microstructure and mechanical properties of laser melting deposited γ-TiAl intermetallic alloys. Mater Sci Eng A 2007;466:187–94. doi:10.1016/j.msea.2007.02.073.

[20] Qu HP, Li P, Zhang SQ, Li A, Wang HM. The effects of heat treatment on the microstructure and mechanical property of laser melting deposition γ-TiAl intermetallic

alloys. Mater Des 2010;31:2201–10.

[21] Das M, Bhattacharya K, Dittrick SA, Mandal C, Balla VK, Sampath Kumar TS, et al. In situ synthesized TiB-TiN reinforced Ti6Al4V alloy composite coatings: Microstructure, tribological and in-vitro biocompatibility. J Mech Behav Biomed Mater 2014;29:259–71. doi:10.1016/j.jmbbm.2013.09.006.

[22] Hao H, Jiang W, Xie G, Zhang G, Lu Y, Zhang J, et al. Microstructure and grain orientation evolution of a specially shaped shroud during directional solidification process. Prog Nat Sci Mater Int 2013;23:211–5. doi:10.1016/j.pnsc.2013.03.007.

[23] D'Souza N, Newell M, Devendra K, Jennings P a., Ardakani MG, Shollock B a. Formation of low angle boundaries in Ni-based superalloys. Mater Sci Eng A 2005;413–414:567–70. doi:10.1016/j.msea.2005.08.188.

[24] Newell M, Devendra K, Jennings PA, D'Souza N. Role of dendrite branching and growth kinetics in the formation of low angle boundaries in Ni–base superalloys. Mater Sci Eng A 2005;412:307–15. doi:10.1016/j.msea.2005.09.030.

[25] McCullough C, Valencia J., Levi C., Mehrabian R. Phase equilibria and solidification in Ti-Al alloys. Acta Metall 1989;37:1321–36. doi:10.1016/0001-6160(89)90162-4.

[26] Sankaran A, Bouzy E, Fundenberger JJ, Hazotte A. Texture and microstructure evolution during tempering of gamma-massive phase in a TiAl-based alloy. Intermetallics 2009;17:1007–16. doi:10.1016/j.intermet.2009.05.001.

[27] Schloffer M, Iqbal F, Gabrisch H, Schwaighofer E, Schimansky FP, Mayer S, et al. Microstructure development and hardness of a powder metallurgical multi phase γ-TiAl based alloy. Intermetallics 2012;22:231–40. doi:10.1016/j.intermet.2011.11.015.

[28] Rabe M, Verdes D, Seeger S. Understanding protein adsorption phenomena at solid surfaces. Adv Colloid Interface Sci 2011;162:87–106. doi:10.1016/j.cis.2010.12.007.

[29] Wahlgren M, Arnebrant T. Protein adsorption to solid surfaces. Trends Biotechnol 1991;9:201–8. doi:10.1016/0167-7799(91)90064-O.

[30] Clark GC, Williams DF. The effects of proteins on metallic corrosion. Biomed Mater Res 1982;16:125–34. doi:10.1002/jbm.820160205.

[31] Hiromoto S, Onodera E, Chiba A, Asami K, Hanawa T. Microstructure and corrosion behaviour in biological environments of the new forged low-Ni Co-Cr-Mo alloys. Biomaterials 2005;26:4912–23. doi:10.1016/j.biomaterials.2005.01.028.

[32] Hang R, Ma S, Ji V, Chu PK. Corrosion behavior of NiTi alloy in fetal bovine serum. Electrochim Acta 2010;55:5551–60. doi:10.1016/j.electacta.2010.04.061.

[33] Wang Y, Shi L, Duan D, Li S, Xu J. Tribological properties of Zr61Ti2Cu25Al12 bulk metallic glass under simulated physiological conditions. Mater Sci Eng C Mater Biol Appl 2014;37:292–304. doi:10.1016/j.msec.2014.01.016.

[34] Julong D. Introduction to Grey System Theory. J Grey Syst 1989;1:1–24.

[35] Mantrala KM, Das M, Balla VK, Rao CS, Kesava Rao VVS. Additive Manufacturing of Co-Cr-Mo Alloy: Influence of Heat Treatment on Microstructure, Tribological, and Electrochemical Properties. Front Mech Eng 2015;1:1–7. doi:10.3389/fmech.2015.00002.

LIST OF TABLE CAPTIONS

Table 1 Composition, hardness and grain misoirentation of EBM processed γ-TiAl in as-deposited (AD) and hot isostatic pressed (HIPed) conditions.

Table 2 Results of *in vitro* corrosion testing performed on EBM processed γ-TiAl samples.

Table 3 Grey relational analysis of *in vitro* wear and corrosion performance of EBM processed γ-TiAl alloy. G: grade; O: order.

LIST OF FIGURE CAPATIONS

Fig. 1 SEM-BSE microstructures of EBM processed γ-TiAl: (a) as-deposited, (b) HIPed.

Fig. 2 (a, b) Pole figures and EBSD maps, (c, d) dislocation maps (blue regions are dislocation free) of as-deposited γ-TiAl (a, c), HIPed γ-TiAl (b, d).

Fig. 3 X-ray diffractograms of the γ-TiAl power, as-deposited (AD) γ-TiAl samples and HIPed γ-TiAl samples.

Fig. 4 Tafel plots of the samples tested in Hank's solution (a) without fetal bovine serum (FBS), (b) with 10% FBS. AD: as-deposited; HIPed: hot isostatically pressed; ZCP: zero current potential; E_b: breakdown potential.

Fig. 5 Typical surface morphological features after corrosion testing in Hank's solution with FBS (a) as-deposited, (b) HIPed.

Fig. 6 *In vitro* wear rate of EBM processed γ-TiAl samples in as-deposited (AD) and HIPed condition. * indicates $p \leq 0.001$.

Fig. 7 Wear track morphologies of different γ-TiAl samples. (a,b) tested in Hank's without FBS, (c,d) tested in Hank's with FBS. (a, c) as-deposited, (b, d) HIPed.

Fig. 8 *In vitro* cell proliferation on EBM processed γ-TiAl samples in as-deposited (AD) and hot isostatically pressed (HIPed) conditions.

Fig. 9 Morphological characteristics of NIH3T3 cells on CP-Ti and EBM processed γ-TiAl samples in as-deposited (AD) and HIPed conditions: (a) after 3 days, (b) after 5 days, (c) after 7 days.

Table 1 Composition, hardness and grain misoirentation of EBM processed γ-TiAl in as-deposited (AD) and hot isostatic pressed (HIPed) conditions.

	Powder	**AD**	**HIPed**
Density (%)	–	~ 99.0	~ 99.7
		Overall composition (at. %)	
Al	52.34 ± 0.82	51.21 ± 0.51	50.61 ± 0.71
Cr	2.04 ± 0.14	2.45 ± 0.40	2.35 ± 0.24
Nb	1.92 ± 0.10	2.14 ± 0.13	2.24 ± 0.24
Ti	43.74 ± 0.90	44.19 ± 0.62	44.80 ± 0.63
		Hardness, HV0.3	
XY-surface		347 ± 7	369 ± 7
YZ-surface		371 ± 11	364 ± 8
XZ-surface		391 ± 14	378 ± 7
Average	431 ± 13	370 ± 22	370 ± 9
		Grain misorientation (%)	
2° to 5°	–	41.6	11.7
5° to 15°		3.7	1.9
> 15°		54.7	86.4

Table 2 Results of *in vitro* corrosion testing performed on EBM processed γ-TiAl samples.

Sample	**E_{corr} (mV vs SCE)**		**I_{corr} (μA)**		**Passive range (mV)**	
	Hank's	Hank's + 10% FBS	Hank's	Hank's + 10% FBS	Hank's	Hank's + 10% FBS
As-deposited	– 182	– 208	0.002	0.496	1221	Passive
Hot isostatically pressed	– 87	– 262	0.103	0.005	914	458
CP-Ti	– 211	– 476	0.330	0.003	Passive	Passive

Table 3 Grey relational analysis of *in vitro* wear and corrosion performance of EBM processed γ-TiAl alloy. G: grade; O: order.

Sample	Corrosion only				Wear only				Overall			
	HBSS		HBSS + FBS		HBSS		HBSS + FBS		HBSS		HBSS + FBS	
	G	O	G	O	G	O	G	O	G	O	G	O
CP-Ti	0.33	3	0.67	2	–	–	–	–	–	–	–	–
AD γ-TiAl	0.70	2	0.67	2	0.33	2	1.00	1	0.57	2	0.78	1
HIPed γ-TiAl	0.81	1	0.85	1	1.00	1	0.33	2	0.87	1	0.68	2

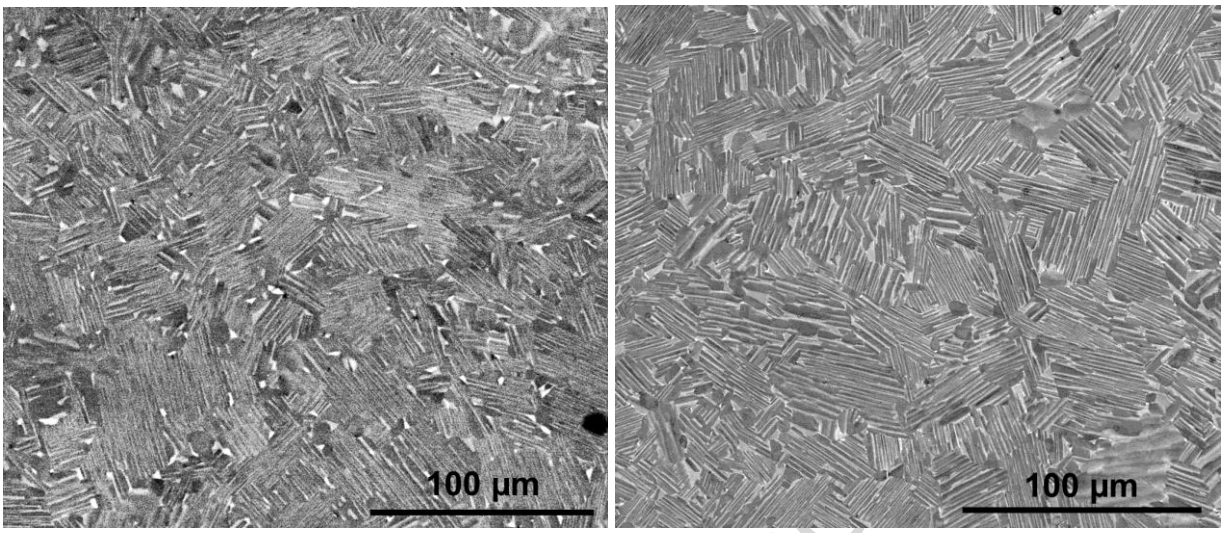

(a) (b)

Fig. 1 SEM-BSE microstructures of EBM processed γ-TiAl: (a) as-deposited, (b) HIPed.

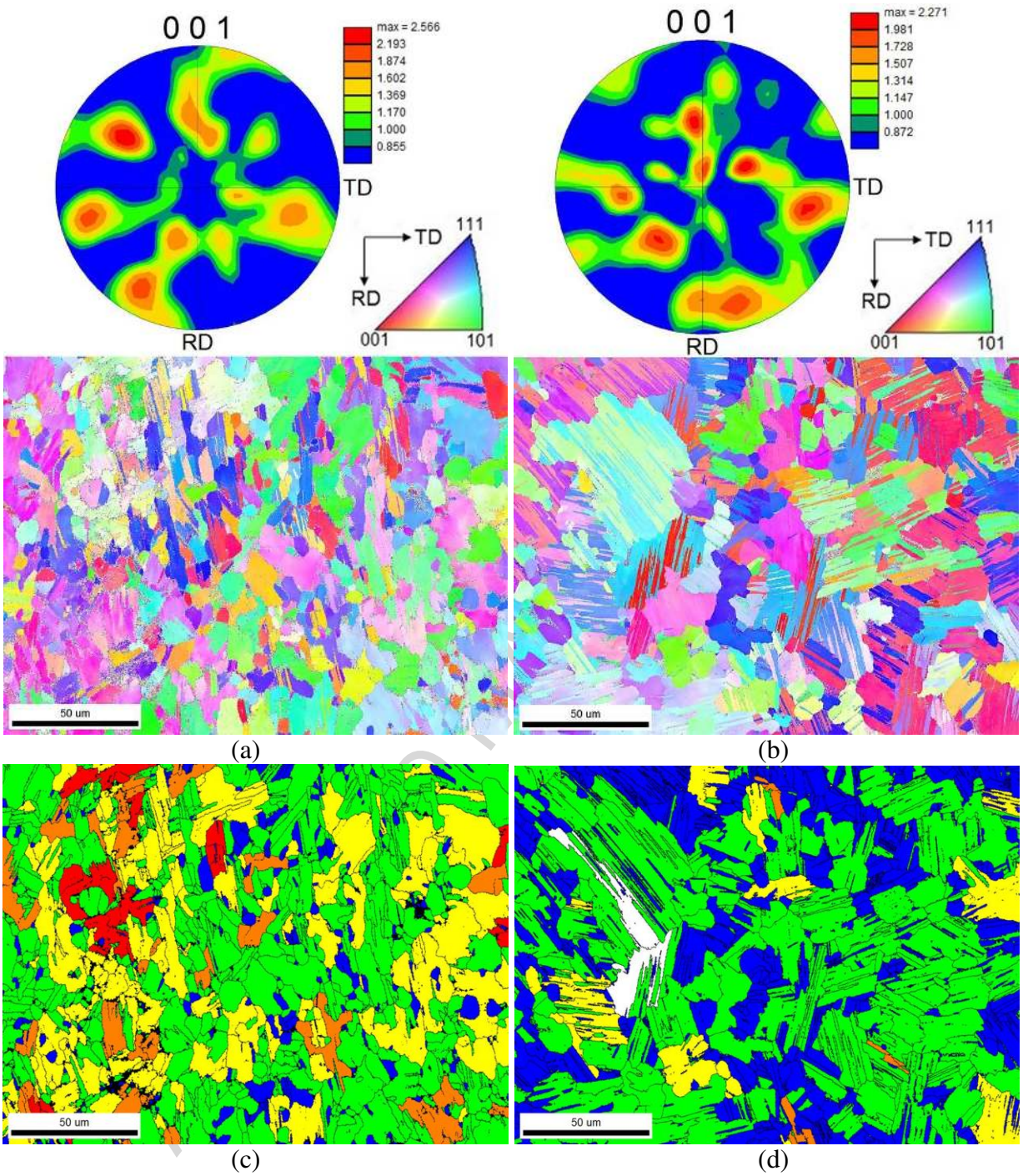

Fig. 2 (a, b) Pole figures and EBSD maps, (c, d) dislocation maps (blue regions are dislocation free) of as-deposited γ-TiAl (a, c), HIPed γ-TiAl (b, d).

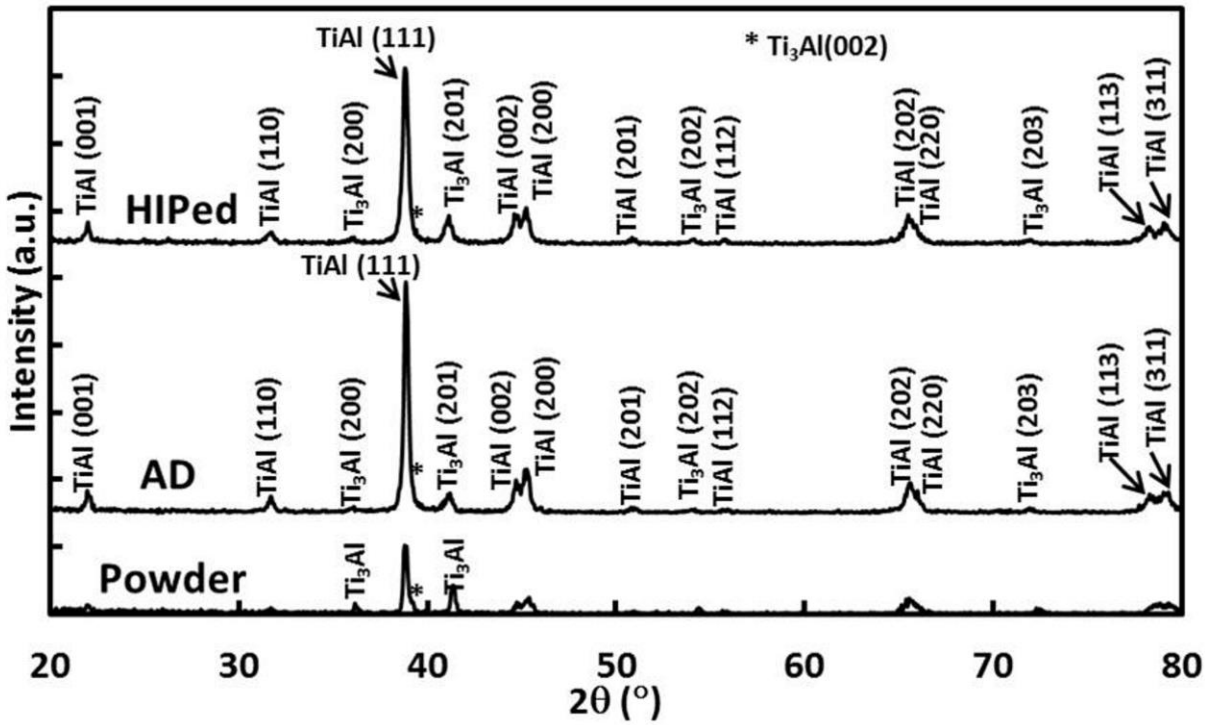

Fig. 3 X-ray diffractograms of the γ-TiAl power, as-deposited (AD) γ-TiAl samples and HIPed γ-TiAl samples.

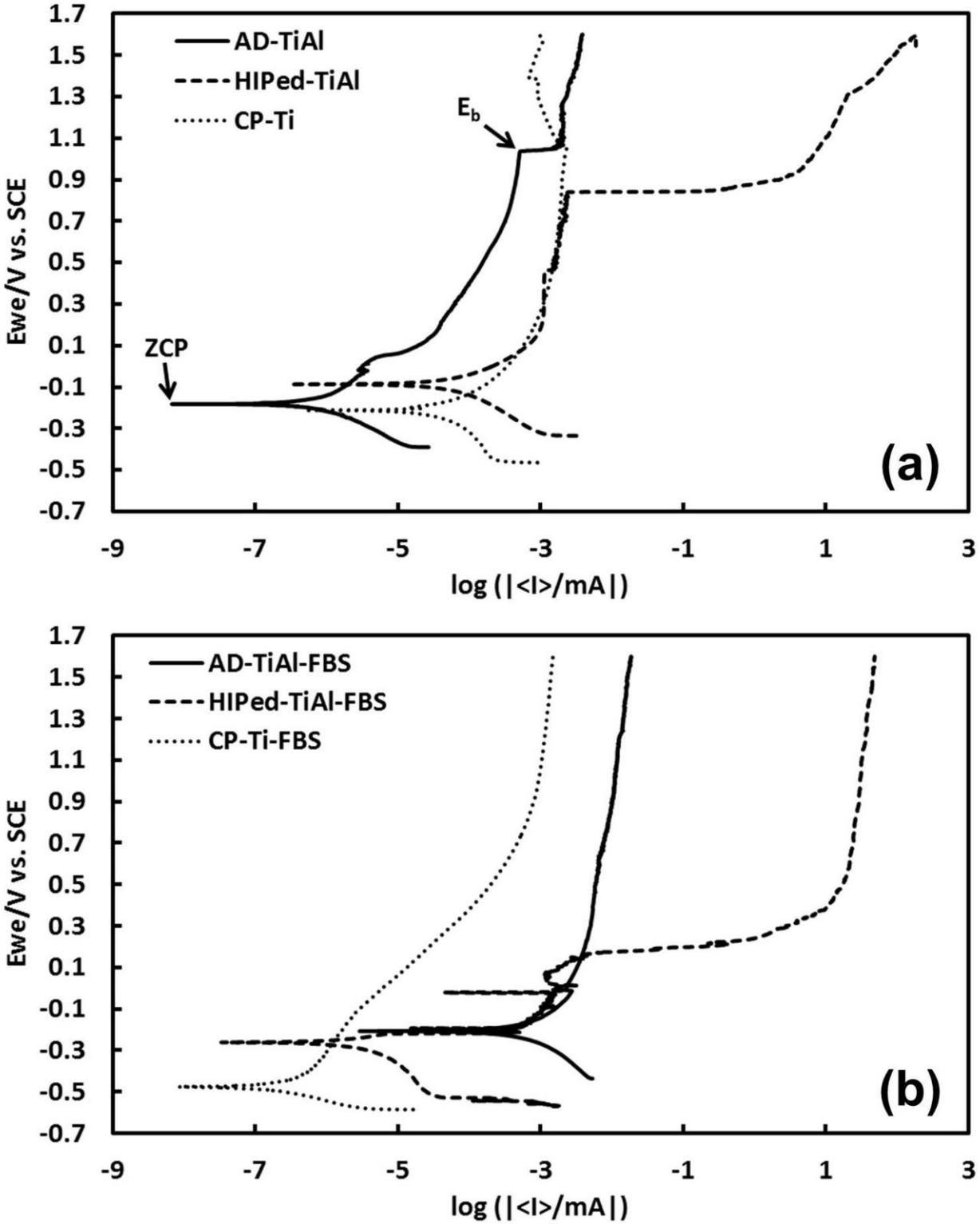

Fig. 4 Tafel plots of the samples tested in Hank's solution (a) without fetal bovine serum (FBS), (b) with 10% FBS. AD: as-deposited; HIPed: hot isostatically pressed; ZCP: zero current potential; E_b: breakdown potential.

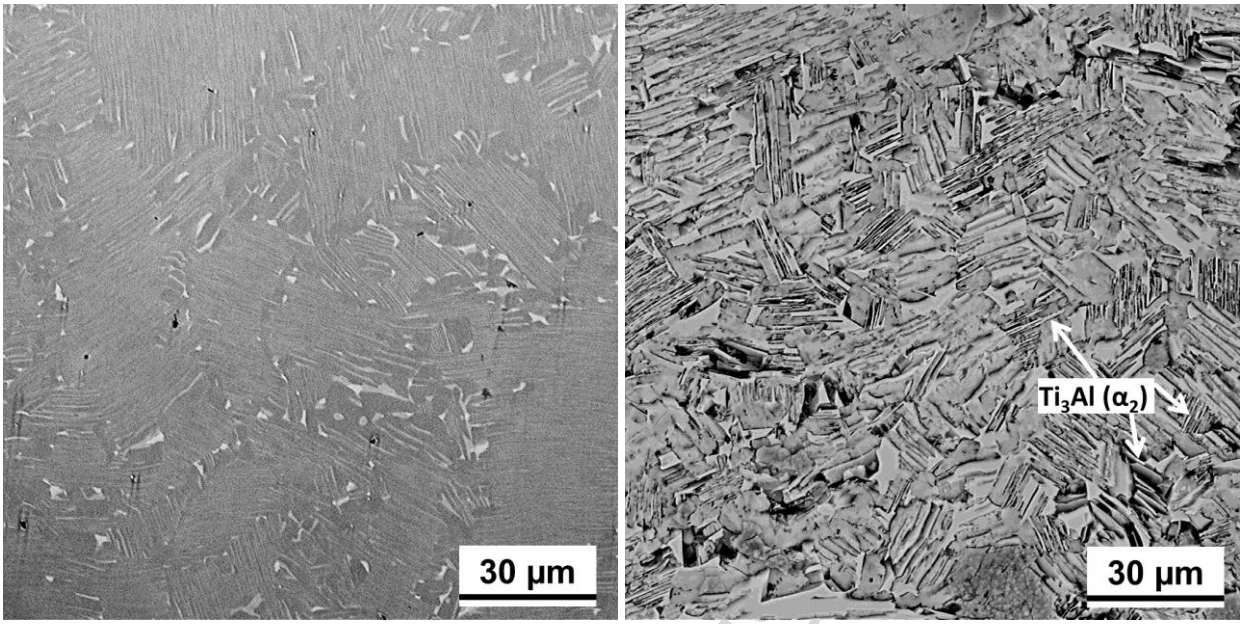

(a) (b)

Fig. 5 Typical surface morphological features after corrosion testing in Hank's solution with FBS (a) as-deposited, (b) HIPed.

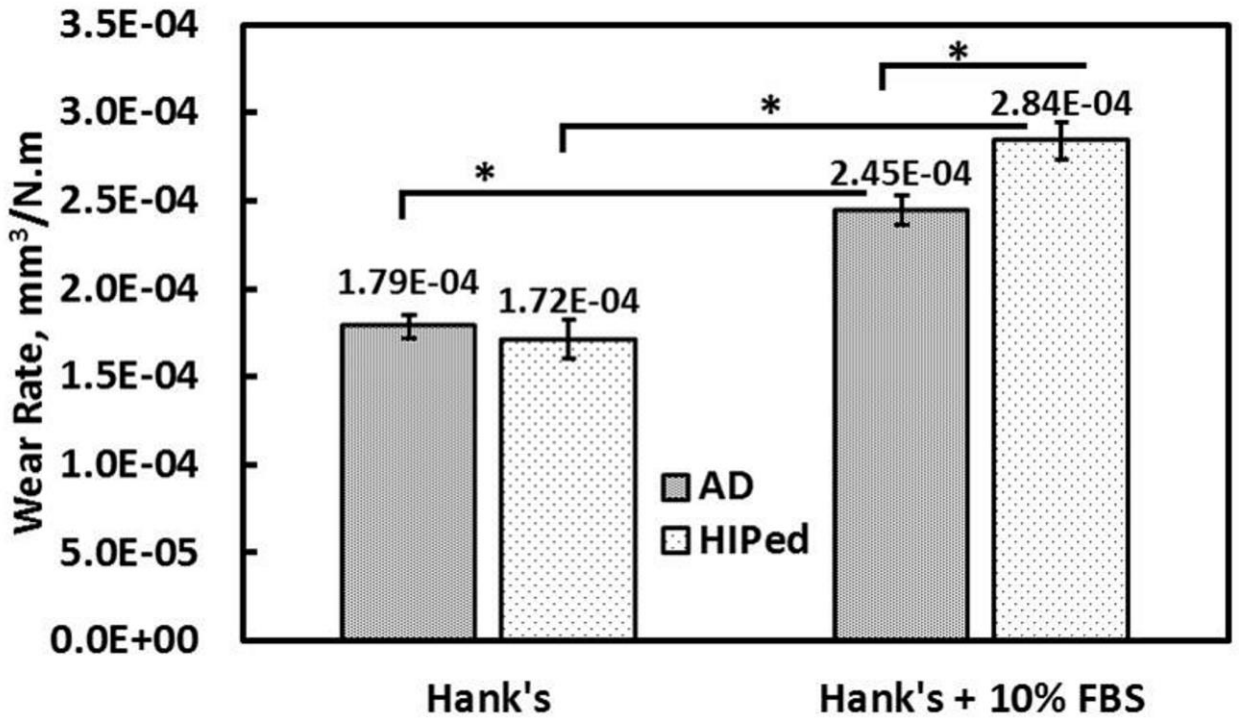

Fig. 6 *In vitro* wear rate of EBM processed γ-TiAl samples in as-deposited (AD) and HIPed condition. * indicates $p \leq 0.001$.

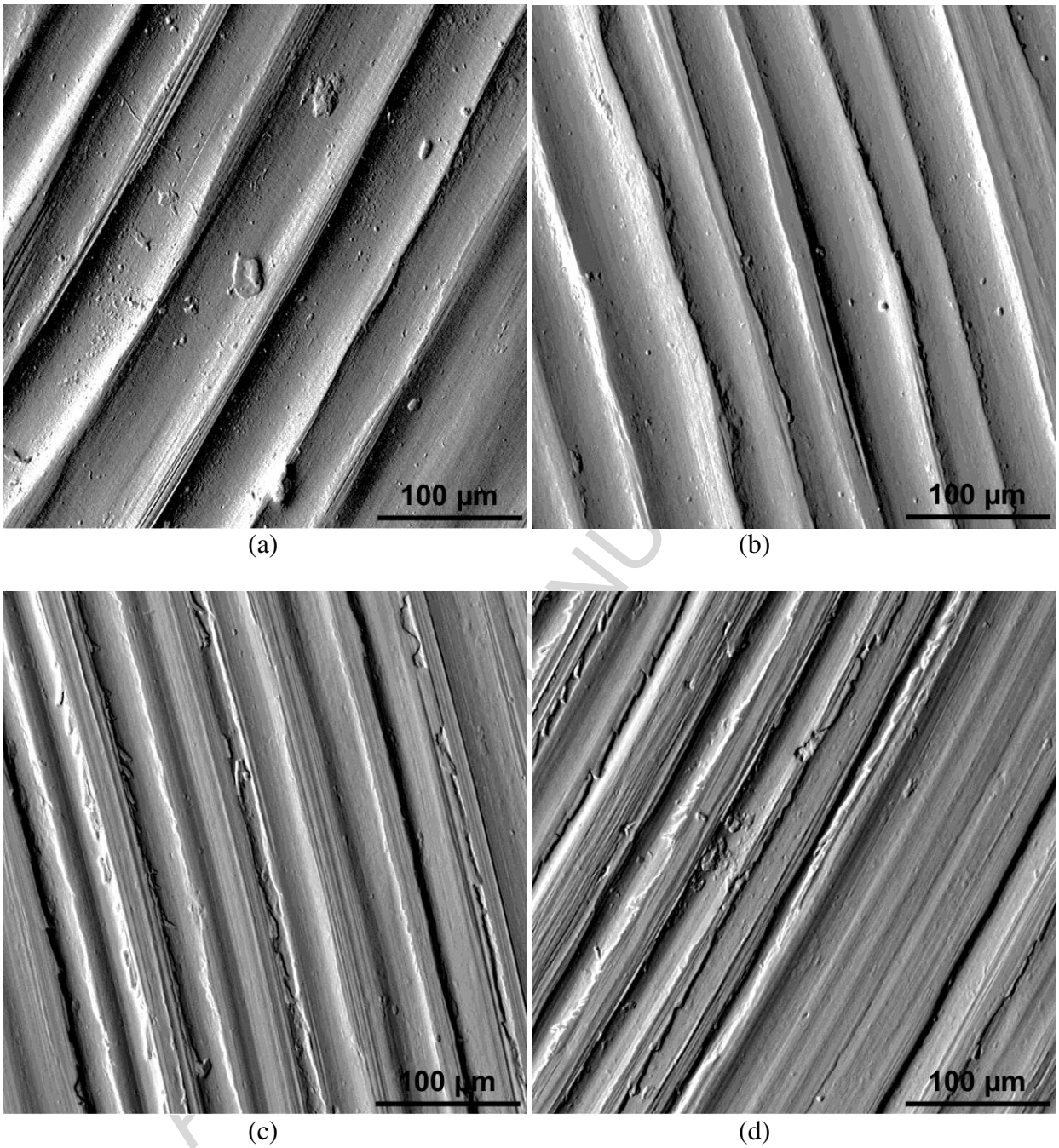

Fig. 7 Wear track morphologies of different γ-TiAl samples. (a,b) tested in Hank's without FBS, (c,d) tested in Hank's with FBS. (a, c) as-deposited, (b, d) HIPed.

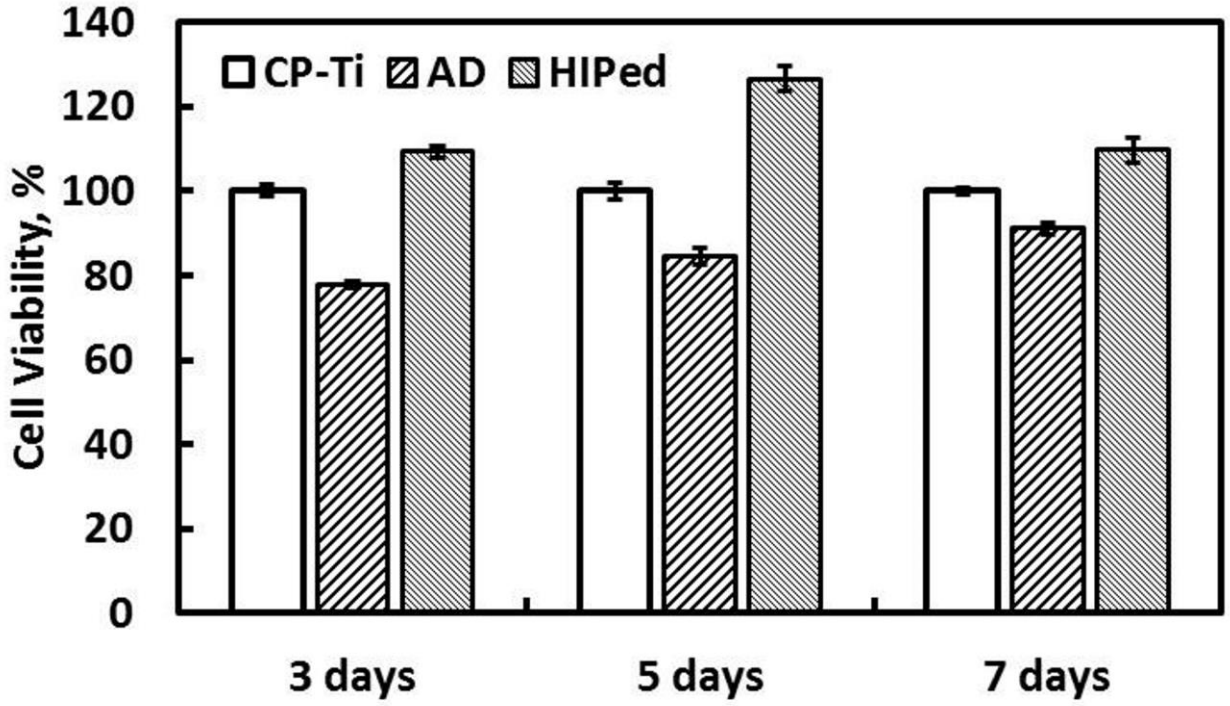

Fig. 8 *In vitro* cell proliferation on EBM processed γ-TiAl samples in as-deposited (AD) and hot isostatically pressed (HIPed) conditions.

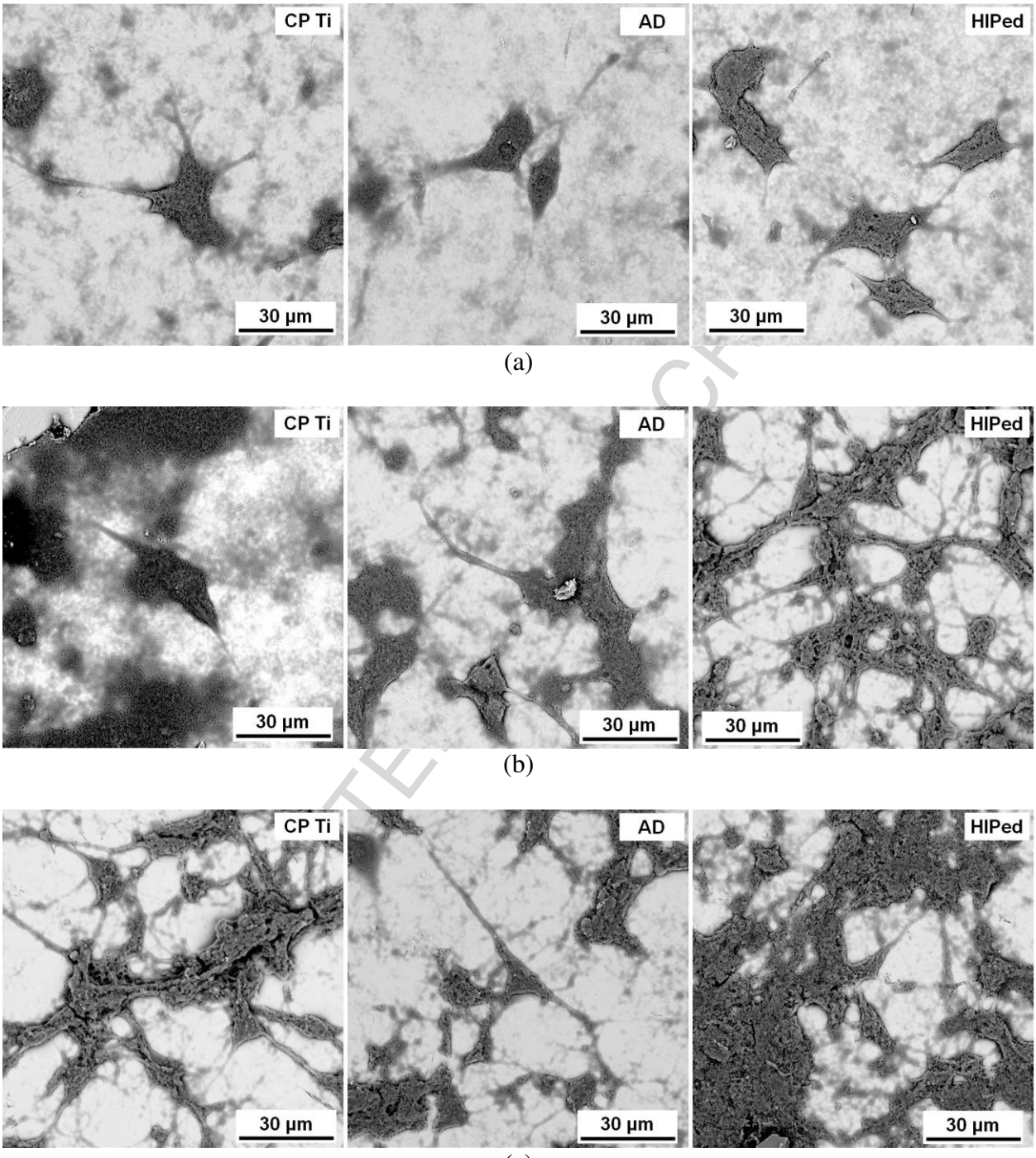

Fig. 9 Morphological characteristics of NIH3T3 cells on CP-Ti and EBM processed γ-TiAl samples in as-deposited (AD) and HIPed conditions: (a) after 3 days, (b) after 5 days, (c) after 7 days.

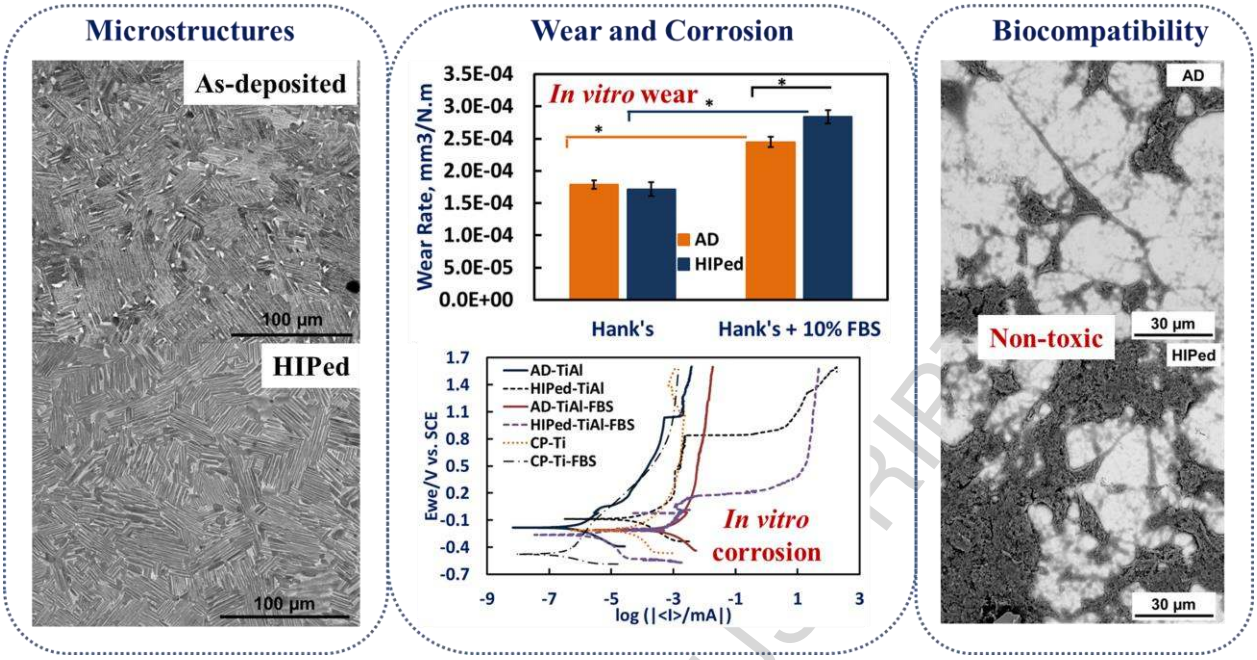

Graphical abstract

Research highlights

- The electron beam melted γ-TiAl alloy showed potential for use in biomedical implants.
- Hot isotatic pressing of electron beam melted γ-TiAl alloy improved its *in vitro* corrosion reistance and cell viability (up to 42%).
- The alloy exhibited similar *in vitro* wear resistance in as-processed and hot isostatically pressed conditions.
- The presence of fetal bovine serum increased the wear rate of γ-TiAl alloy by 65%.
- The electron beam melted γ-TiAl alloy is non-toxic and its *in vitro* cell-material interactions are comparable to that of titanium.